http://www.journalmt.com

Deformation and Velocity Wave Propagation in a Thin Isotropic Plate

Frantisek Klimenda (0000-0001-7937-3755)[1], Blanka Skocilasova (0000-0001-8242-3231)[1], Jan Skocilas (0000-0002-1845-2000)[2], Josef Soukup (0000-0001-8325-3529)
[1]Faculty of Mechanical Engineering, J. E. Purkyne University in Usti nad Labem. Pasteurova 3334/7, 400 01 Usti nad Labem. Czech Republic. E-mail: frantisek.klimenda@ujep.cz, blanka.skocilasova@ujep.cz
[2]Faculty of Mechanical Engineering, Czech Technical University in Prague, 4 Technicka, Prague 166 07, Czech Republic. E-mail: jan.skocilas@fs.cvut.cz

The propagation and velocity of the deformation wave in the thin isotropic plate is investigated. The deformation is induced by the stroke of impact body onto the facial surface of the plate. The plate is supported perpendicularly. The excitation of the plate oscillation is initialized by a unit force (Heaviside's jump). The impact body has a rounded facet by radius c = 2.5 mm. Hook's material model and Kirchhoff's and Flüegge's geometric model have been investigated. The analytical solutions for both models are presented. The MATLAB script has been assembled to solve material and geometrical models. The results were compared for two selected points on the surface of the plate. Plate deformation was recorded at two points T1 (at a distance of 20 mm from the impact location on the x axis) and T2 (at a distance of 20 mm from the impact location on the y axis).

1 Introduction

The problem of plates vibration, especially the vibration of thin plates, has been solved for more than 200 years. There is still no comprehensive theory available that would satisfactorily solve all the issues associated with plates vibration. Plates, especially thin ones, are currently found in many areas of human activity. This is mainly mechanical engineering (construction of cars, planes, ships, containers, rockets, tanks, etc.), civil engineering (construction of bridges, buildings, concrete silos, etc.), possibly also in other fields of human activity (boards sports, agriculture, chemical industry etc.).

Plates are structural elements bounded by two parallel planes (surfaces). The plate can be bounded by a peripheral surface or by peripheral edge (e.g., a cylindrical shell). The distance between the parallel surfaces is the thickness of the plate (h). According to the ratio a/h of the typical size of the plate a (edge length) and its thickness h, we divide the plates into:

- Thick, where a/h ≤ 8 to 10. The analysis of such bodies includes all components of stress, strain, and displacement same for three-dimensional solids. The general equations of three-dimensional elasticity are used.

- Membranes, are plates with a/h ratio ≥ 80 to 100. These plates lack bending stiffness.

Lateral loads are transferred by axial tensile and shear forces acting in the middle plane of the plate (membrane forces).

- Thin, which have a ratio of 8 to 10 ≤ a/h ≤ 80 to 100. This type of plates represents the so-called transitional type between thick plates and membranes and forms the most extensive group of plates used. Depending on the ratio w/h of the maximum plate deflection w to its thickness h, the proportion of bending and membrane forces can be different. We divide these plates into two classes according to this ratio:

  - Rigid plates (ratio w/h ≤ 0.2) are flexurally rigid and transmit loads two-dimensionally (by internal bending and torsional moments and transverse shear forces). Midplane deformations and membrane forces are negligible. In practice, the term plate represents a rigid thin plate.

  - Elastic plates (ratio w/h ≥ 0.3). This plate is characterized by lateral deflections are accompanied by

stretching (deformation) of the central surface of the board. It is a combination of rigid plates and membranes. The external load is transmitted by the combined action of internal moments, shear forces and membrane (axial) forces. Plates of this type are often used in the aerospace industry. When the maximal deflection is considerably larger than the thickness of the plate (w/h > 5), the membrane force transfer prevails, and the bending stress can be neglected. The stress is then uniformly distributed over the entire thickness of the plate.

The above division of plates is conditioned mainly by their rheological properties, type of load, boundary conditions, etc. These plates are in practice loaded by static or dynamic forces, usually perpendicular to the surface of the plate. From the point of view of plate damage, dynamic loading is more significant, when the force acts on the plate in a very short time interval (shock load, usually by an impact that has a specific kinetic energy). We divide this impact damage into three basic groups according to the velocity at the impact [1 - 3].

- Low velocities (up to 10 m·s^{-1}). This damage is dependent on the response of the structure (plate), the type of material, the type and geometry of the impact and the residual force. This damage usually does not exhibit on the surface, but inside the body from the residual force. Studies of this damage are focused on impact dynamics, damage mechanics and residual properties of the material after impact, including damage resistance. It is also dependent on the size of the impact test specimen, its stiffness, the stiffness and material properties of the plate, and the initial conditions.

- Medium velocities (from 20 to 100 m·s^{-1}). The extent of damage depends mainly on the weight of the impact (usually flat), a typical example is e.g. a traffic accident, when parts of a car flying away hit other parts of the car at a low final velocity.

- High velocities (ballistic velocities). This damage is mainly used to damage fiber composites in the arsenal industry. We define a high-velocity shock by the ratio of the impact velocity to the velocity of the transverse (pressure) wave. The pressure wave will induce a stress that is greater than the maximum stress required to fracture the composite in a given direction. The response of the material is dependent on the velocity of the wave propagation, not on the velocity of the impact. The response is controlled by the propagation of the wave and not by the velocity of the impact. At low velocity, delamination and crack formation occur in the matrix. At high speed to fiber breakage occurs.

Depending on the rheological properties of the plate, we use different material models (Hooke's, Voight-Kelvin's, Maxwell's, Zener's or generalized Zener's model of a standard body) to solve the problem - see Fig. 1.

These material models are assigned to individual geometric models [4, 5]. The simplest geometric model is Kirchhoff's (considers only vertical displacements and their corresponding inertial effects). Rayleigh's model includes the influence of cross-section rotation and the corresponding inertial effects of the plate. Flüegge's model considers the effect of shear on the resulting vertical displacement. The inclusion of both corrections (Rayleigh and Flüegge) solves the Timoshenko-Mindlin model, which comes closest to reality.

Currently, the attention is paid to solving the propagation of deformations and stress waves in isotropic and orthotropic materials, which allows us to use especially thin structures in mechanical and civil engineering and other fields. When solving this issue, it is important to use suitable material and especially geometric models and appropriately defined boundary conditions. A number of authors deal with the solution [6-10], but this complex issue is not satisfactorily resolved. A number of methods are used for the solution, from analytical or FEM to experimental [11, 12].
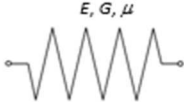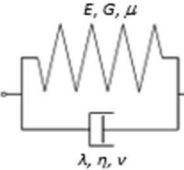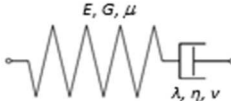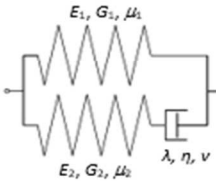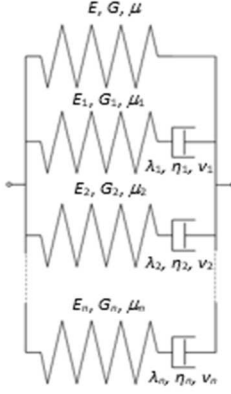
Model	Scheme	Tension
Hooke's model	E, G, μ	$\boldsymbol{\sigma}_i = \mathbf{c}_{ij}\boldsymbol{\varepsilon}_j$
Voight-Kelvin's model	E, G, μ / λ, η, υ	$\boldsymbol{\sigma}_i = \mathbf{b}_{ij}\boldsymbol{\varepsilon}_j + \mathbf{d}_{ij}\dfrac{\partial \boldsymbol{\varepsilon}_j}{\partial t}$
Maxwell's model	E, G, μ / λ, η, υ	$\mathbf{a}_{ij}\boldsymbol{\sigma}_i + \mathbf{c}_{ij}\dfrac{\partial \boldsymbol{\sigma}_i}{\partial t} = \mathbf{d}_{ij}\dfrac{\partial \boldsymbol{\varepsilon}_j}{\partial t}$
Zener's model	E_1, G_1, μ_1 / λ, η, υ / E_2, G_2, μ_2	$\boldsymbol{\sigma}_i + \mathbf{c}_{ij}\dfrac{\partial \boldsymbol{\sigma}_i}{\partial t} = \mathbf{b}_{ij}\boldsymbol{\varepsilon}_j + \mathbf{d}_{ij}\dfrac{\partial \boldsymbol{\varepsilon}_j}{\partial t}$
A generalized Zener's model of a standard body	E, G, μ / E_1, G_1, μ_1 / $\lambda_1, \eta_1, \upsilon_1$ / E_2, G_2, μ_2 / $\lambda_2, \eta_2, \upsilon_2$ / E_n, G_n, μ_n / $\lambda_n, \eta_n, \upsilon_n$	$\boldsymbol{\sigma}_i + \mathbf{c}_{ij}\dfrac{\partial \boldsymbol{\sigma}_i}{\partial t} = \mathbf{b}_{ij}\boldsymbol{\varepsilon}_j + \mathbf{d}_{ij}\dfrac{\partial \boldsymbol{\varepsilon}_j}{\partial t}$

Fig. 1 *Material models of plates (E, G – modulus of elasticity in tension and shear, μ, λ – coefficients of normal and shear viscosity, η, υ Poisson's ratio for elastic and viscous component, a_{ij}, b_{ij}, c_{ij}, d_{ij} – matrix of coefficients, εj – deformation vector)*

2 Analytical solution of thin plate

Analytical solution of free oscillation and non-stationary tension of thin plates ($h << (a$ - length, b – width), middle plane bisects the thickness of the plate) is based on motion equations, mathematical models of these plates, which are independent of the material description. When solving a specific problem, it is necessary to supplement these motion equations with a description of the material properties of the plate and consider the type of its load, including initial and boundary conditions [13, 14].

When solving plates, we arise from their rheological and geometric properties. We assume that the plate is symmetrical in three planes. We further assume that

- Longitudinal elements of the middle plane do not change their length, even after deformation of the plate, so they have zero normal strains and zero normal stresses

- Displacements of points lying outside the middle plane in the directions of the x and y axes are directly proportional to the distance from this plane –> linear dependence of the stress in these directions.

Thus, the solution equations contain nine independent constants. Furthermore, we assume small deformations of the plate under load and stress directions that are different from the directions of symmetry of the material axes. The physical equations that describe the relationship between stress and strain components for a 3D continuum can be simply written in the form of a generalized Hooke's law in the form:

$$\sigma_{ik} = c_{iklm} \cdot \varepsilon_{lm} \text{ for } i, k, l, m = 1, 2, 3 \tag{1}$$

Where:

σ_{ik}…Components of the normal and shear stress tensor [Pa],

c_{iklm}…Stiffness coefficients [Pa],

εim…Components of the specific deformation tensor [-].

By solving equation (1), we get 81 stiffness coefficients, which, however, are generally not independent. If we assume only force that act between the elementary surfaces with a continuous stress distribution, then the elementary forces from the normal stresses acting on the walls of the element will pass through its center of gravity (with an infinitesimally small deviation). From this follows the law of combined shear stresses. Of the original 81 coefficients, only 36 will remain independent (it is valid $c_{iklm} = c_{kilm} = c_{ikml} = c_{kiml}$, $c_{iklm} = c_{lmik}$, it follows that $\sigma_{ik} = \sigma_{ki}$ and analogously $\varepsilon_{lm} = \varepsilon_{ml}$, for $i \neq k$ and $l \neq m$).

Using the above mentioned and abbreviated indices, Hooke's law can be written in a simplified form.

$$\sigma_i = c_{ij} \, \varepsilon_j \text{ for } i, j = 1, 2, 3, 4, 5, 6 \tag{2}$$

If the material has three mutually perpendicular planes of symmetry intersecting in three intersections, which form three mutually perpendicular material axes, and their direction is identical to the direction of the coordinate axes, then $c_{ij} = 0$, if one of the indices $i, j = 4, 5, 6$. Then the number of independent coefficients is reduced to 12. We assume the validity of the superposition principle, then we reduce the number of these coefficients by applying Betti's theorem to 9. In our case, we consider the isotropic material.

If the coordinate axes coincide with the material axes, the relationship between the stress and strain components can be expressed as:

$$\begin{bmatrix} \sigma_x \\ \sigma_y \\ \sigma_z \\ \tau_{yz} \\ \tau_{xz} \\ \tau_{xy} \end{bmatrix} = \begin{bmatrix} c_{11} & c_{12} & c_{13} & 0 & 0 & 0 \\ c_{21} & c_{22} & c_{23} & 0 & 0 & 0 \\ c_{31} & c_{32} & c_{33} & 0 & 0 & 0 \\ 0 & 0 & 0 & c_{44} & 0 & 0 \\ 0 & 0 & 0 & 0 & c_{55} & 0 \\ 0 & 0 & 0 & 0 & 0 & c_{66} \end{bmatrix} \cdot \begin{bmatrix} \varepsilon_x \\ \varepsilon_y \\ \varepsilon_z \\ \gamma_{yz} \\ \gamma_{xz} \\ \gamma_{xy} \end{bmatrix} \tag{3}$$

Or in the inverse form of equation:

$$\varepsilon_j = s_{ij} \cdot \sigma_i \text{ for } i, j = 1, 2, 3, 4, 5, 6 \tag{4}$$

Where:

s_{ij}…Matrix of elastic modules [-].

The solution of equations (3), (4) is given, for example, in the literature [13, 15, 16], where, using Betti's theorem, relations between elastic constants for orthotropic material are obtained.

$$\mu_{xy} E_y = \mu_{yx} E_x \qquad \mu_{zy} E_y = \mu_{yz} E_z \qquad \mu_{xz} E_z = \mu_{zx} E_x. \tag{5}$$

Assuming:

$$\sigma_z = 0 \quad \gamma_{xz} = 0 \quad \gamma_{yz} = 0 \tag{6}$$

From equations (3, 4, 5, 6) the relations for deformation of the plate are derived:

$$\varepsilon_x = \frac{\partial u}{\partial x} = \frac{\sigma_x}{E_x} - \frac{\mu_{yx}}{E_y}\sigma_y - \frac{\mu_{zx}}{E_z}\sigma_z \quad \varepsilon_y = \frac{\partial v}{\partial y} = \frac{\sigma_y}{E_y} - \frac{\mu_{xy}}{E_x}\sigma_x - \frac{\mu_{zy}}{E_z}\sigma_z \quad \varepsilon_z = \frac{\partial v}{\partial z} = \frac{\sigma_z}{E_z} - \frac{\mu_{xz}}{E_x}\sigma_x - \frac{\mu_{yz}}{E_y}\sigma_y$$

$$\gamma_{yz} = \frac{\partial v}{\partial z} + \frac{\partial w}{\partial y} = \frac{\tau_{yz}}{G_{yz}} \qquad \gamma_{xz} = \frac{\partial u}{\partial z} + \frac{\partial w}{\partial x} = \frac{\tau_{xz}}{G_{xz}} \qquad \gamma_{xy} = \frac{\partial u}{\partial y} + \frac{\partial v}{\partial x} = \frac{\tau_{xy}}{G_{xy}} \tag{7}$$

If we assume small deformations, we can express relation between the Kirchhoff and Rayleigh model:

$$\frac{\partial w}{\partial x} = \varphi_x \qquad \frac{\partial w}{\partial y} = \varphi_y \tag{8}$$

And for the Flüegge and Timoshenko-Mindlin models, which consider the effect of shearing forces on plate deflection:

$$\frac{\partial w}{\partial x} = \varphi_x + \gamma_{xz} \qquad \frac{\partial w}{\partial y} = \varphi_y + \gamma_{yz} \tag{9}$$

Where:

φ_x, φ_y…The angle of rotation of the cross-sections of the plate about the x and y axes [-],

γ_{xy}, γ_{yz}…Shear deformations [-].

With small deformations and the assumption of

conservation the planar cross sections of the plate element, it is possible to write for displacements in the directions of the x and y axes:

$$\sigma_x = \frac{E_x}{1-\mu_{xy}\mu_{yx}}\left(\varepsilon_x + \mu_{yx}\varepsilon_y\right) \qquad \sigma_y = \frac{E_y}{1-\mu_{xy}\mu_{yx}}\left(\varepsilon_y + \mu_{xy}\varepsilon_x\right) \qquad \tau_{xy} = G_{xy}\gamma_{xy} \qquad (11)$$

From the given relations it follows that the components of the stress tensor σ_x, σ_y, τ_{xy} at any point of the plate A (x, y, z) are a linear function of z, then in the median plane $z = 0$, these stresses are zero.

Assuming small strains, the components of the strain tensor are functions of the displacement vector v in the Cartesian coordinate system. If we further assume that $\varepsilon_z = 0$, then the vertical displacement w of the general point of the median surface is not a function of z. Then:

$$w = w (x, y, t) \qquad (12a)$$

Similarly, from equations (7) we get for displacements u, resp. v relationships:

$$u = u (x, y, z, t) \quad v = v (x, y, z, t) \qquad (12b)$$

The above equations describe the deformation geometry of the thin plate and the basic stress, from which we can derive the equations of motion for all considered basic mathematical models of the thin orthotropic plate.

After determining the mechanical properties of the plate material (physical equations) and after analyzing the geometry of the deformation of the thin plate based on the accepted assumptions (geometrical equations) and their interrelationship (i.e. established relations for stress components as a function of displacements), the conditions of the dynamic balance of forces and moments are determined acting on the plate element. The effects acting on this element form a general spatial system of forces for which six equations of motion are valid. Three equations of motion are component equations written in the direction of the x, y, z coordinate axes and three moment equations written to the x', y', z' axes, which are parallel to the coordinate axes and pass through the center of gravity of the element.

The motion equations are written for an element

$$u = -z\varphi_x \qquad v = -z\varphi_y \qquad (10)$$

By modifying the above equations and substituting into (7), the inverse relations are derived:

with edges $dx \times dy$ in the directions of the x and y axes. In the direction of the z axis we consider the dimension of the plate of thickness h (Fig. 2).
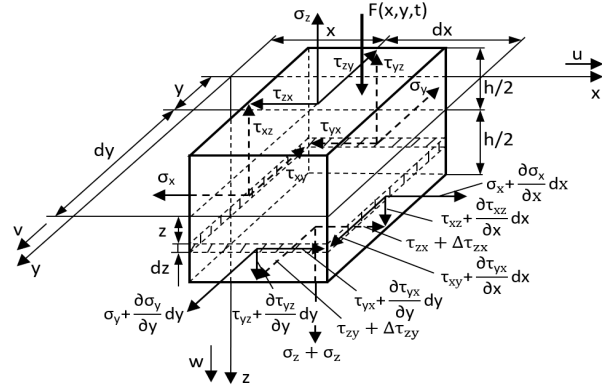

Fig. 2 *Forces and stresses acting on the plate element*

In the theory of thin plates, we usually formulate motion equations in integral form for the element $dx \times dy \times h$, i.e. using specific shear forces and bending and torque moments, referred to a unit of length and thus in a finite area $1 \times h$ (Fig. 3).
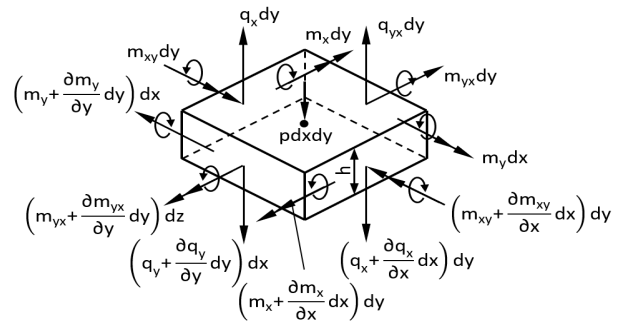
Fig. 3 *Forces and moments acting on the plate element*

After substitution and adjustments, we will get the specific moments:

$$m_x = \frac{M_x}{dy} = \int_{-h/2}^{h/2} \sigma_x z\,dz \qquad m_y = \frac{M_y}{dx} = \int_{-h/2}^{h/2} \sigma_y z\,dz \qquad m_{xy} = \frac{M_{xy}}{dx} = \int_{-h/2}^{h/2} \tau_{xy} z\,dz \qquad (13)$$

And for specific shear forces the relations:

$$q_{yz} = \frac{Q_{yz}}{dx} = \int_{-h/2}^{h/2} \tau_{yz}\,dz \qquad q_{xz} = \frac{Q_{xz}}{dy} = \int_{-h/2}^{h/2} \tau_{xz}\,dz$$

$$(14)$$

$$q_{yx} = \frac{Q_{yx}}{dx} = \int_{-h/2}^{h/2} \tau_{yx}\,dz \qquad q_{xy} = \frac{Q_{xy}}{dy} = \int_{-h/2}^{h/2} \tau_{xy}\,dz$$

To write the equations of motion, we determine the moments of inertia of the mass to the axes that pass through the center of gravity of the element (x', y') - (Fig. 4).

Fig. 4 *Determination of moments of inertia of the mass of the element*
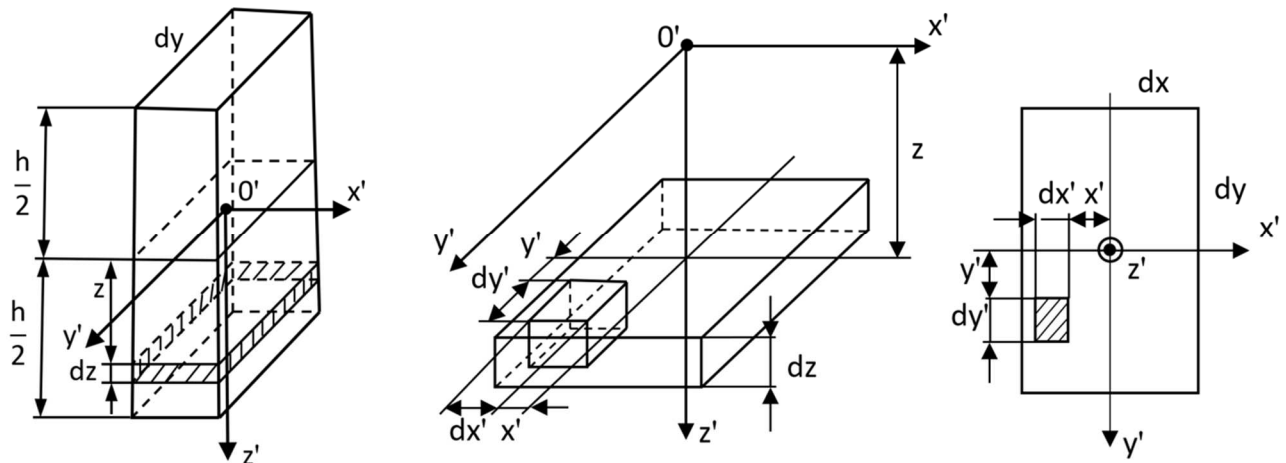
Assuming that $h >> dx$, dy, we determine the mass moment of inertia of the plate element from the relations:

$$J_{x'} = J_{y'} = \int_{-h/2}^{h/2} \rho z^2 dx dy dz = \frac{\rho h^3 dx dy}{12}$$

$$J_{z'} = \int_{-dx'/2}^{dx'/2} \int_{-dy'/2}^{dy'/2} \int_{-h/2}^{h/2} \rho h(x'^2 + y'^2) dx' dy' dz = \frac{\rho h (dx^3 + dy^3)}{12}$$

(15)

If the above assumptions are valid, the stress courses τ_{xy} and τ_{yx} depending on z are analogous to the stress σ_x and σ_y. They therefore have a linear course and are asymmetric with respect to the z coordinate.

For stresses after adjustments, we get relations:

$$\frac{\partial}{\partial x} \int_{-h/2}^{h/2} \tau_{xz} dz + \frac{\partial}{\partial y} \int_{-h/2}^{h/2} \tau_{yz} dz + F(x, y, t) = \rho h \frac{\partial^2 w}{\partial t^2}$$

$$-\frac{\partial}{\partial y} \int_{-h/2}^{h/2} \sigma_y z dz - \frac{\partial}{\partial x} \int_{-h/2}^{h/2} \tau_{xy} z dz + \int_{-h/2}^{h/2} \tau_{yz} dz = \frac{\rho h^3 \partial^2 \varphi_y}{12 \partial t^2}$$

$$-\frac{\partial}{\partial x} \int_{-h/2}^{h/2} \sigma_x z dz - \frac{\partial}{\partial y} \int_{-h/2}^{h/2} \tau_{yx} z dz + \int_{-h/2}^{h/2} \tau_{xz} dz = \frac{\rho h^3 \partial^2 \varphi_x}{12 \partial t^2}$$

$$-\int_{-h/2}^{h/2} \tau_{yx} dz + \int_{-h/2}^{h/2} \tau_{xy} dz = 0$$

(16)

The equality of the combined stresses $\tau_{yx} = \tau_{xy}$ follows from the last moment equation mentioned above. Three equations of motion remain, which are valid for the general considered motion of the element and, in addition to displacements, also consider its rotation. These equations are valid for the Rayleigh and Timoshenko-Mindlin models. For models that neglect the rotational inertia of the element (Kirchhoff and Flüegge) they are further simplified. The equations of motion for the forces and moments acting on the plate element $dx \times dy \times h$ can be expressed in integral form after adjustments:

$$\frac{\partial q_{xz}}{\partial x} + \frac{\partial q_{yz}}{\partial y} + F(x, y, t) = \rho h \frac{\partial^2 w}{\partial t^2}$$

$$q_{xy} - \frac{\partial m_x}{\partial x} - \frac{\partial m_{xy}}{\partial y} = J_\rho \frac{\partial^2 \varphi_x}{\partial t^2} \quad \text{Where:} \quad J_\rho = \frac{\rho h^3}{12} \tag{17}$$

$$q_{yz} - \frac{\partial m_y}{\partial y} - \frac{\partial m_{yx}}{\partial x} = J_\rho \frac{\partial^2 \varphi_y}{\partial t^2}$$

Where:

ϱ…Density [kg.m^{-3}],

F…Excitation force [N],

J_ϱ…The moment of inertia of the mass of the element $dx \times dy \times h$ [Nm].

This case is important for the analysis of the propagation of stress waves. But it is less suitable for the comparison of the theoretical and experimental solution because the point load cannot be practically implemented in the experiment. The external point load always acts in a certain area (rectangular a_F, b_F, circular with radius c, etc.) and the continuous load has different intensity [17-22]. In our case, we compare the analytical solution of wave propagation from shock loading of two geometric models that have one common material model.

In both cases (Kirchhoff, Flüegge) for a plate that is supported around the perimeter is valid that at the point of support there is:

- Vertical displacement $w = w(x, y, t) = 0$

- Bending moment $m_x = m_y = 0$

Stress waves propagate in the plate by free harmonic oscillation with frequency ω.

2.1 Solving geometric models of thin isotropic plates

The paragraph is devoted to the comparison of the propagation of deformations and wave velocities in a thin isotropic plate induced by shock for the Kirchhoff and Flüegge geometric models. In both cases, the Hooke material model is considered. The impact is caused by a body with a circular cross-section (πc^2). The thin plate is supported around the perimeter, the external load is continuous and of constant intensity. The time course of the load is in the form of a Heaviside step function.

2.1.1 Kirchhoff model

The simplest geometric model is the Kirchhoff (mK) model, which considers only vertical displacements and their corresponding inertial effects. An isotropic thin plate is solved without corrections, then $J_\varrho = 0$. The second and third equations (17) then have the character of moment equations of static equilibrium, the influence of moments of inertia is neglected, and effect of rotation of cross sections respectively. The time courses of the deformation of the thin plate, which are caused by the excitation load, are searched for. So, equations (12a) and (12b) are solved. The solution for equations (12a), when excited by a solitary force F_0 is:

$$w(x, y, t) = \frac{16}{abc} \frac{F_0}{\rho h} \sum_{m=1}^{\infty} \sum_{n=1}^{\infty} \frac{J_1(\gamma_{mn} c)}{\gamma_{mn}} \frac{\sin \alpha_n x_F \cos \beta_m y_F}{\omega_{mn}^2} \sin \alpha_n x \sin \beta_m y \sin^2 \frac{\omega_{mn}}{2} t \tag{18}$$

Where:

F_0…Excitation force [N],

J_1…Bessel function of the first kind, first order for the argument $\gamma_{mn} c$ [-],

a, b…Thin plate dimensions [m],

c…The radius of the circle of the applied load body [m],

h…Plate thickness [m],

t…Time [s],

x, y…Coordinates of the resolved point [-],

x_F, y_F…Coordinates of the center of the circular load [-],

α_n, β_m…Constants [-],

γ_{mn}…Constant [-],

ϱ…Density [kg.m^{-3}],

ω_{mn}…Eigen frequency [Hz].

For eigen frequency is valid:

$$\omega_{mn} = (\alpha_n^2 + \beta_m^2) \sqrt{\frac{D}{\rho h}} = (\alpha_n^2 + \beta_m^2) \frac{ch}{\sqrt{12}} \tag{19}$$

Where the stiffness moduli for an isotropic material are $D = D_x = D_y$, elasticity $E = E_x = E_y$ and material viscosity coefficients $\mu = \mu_x = \mu_y$. Then:

$$D = \frac{Eh^3}{12(1-\mu^2)} = D_x = D_y \qquad \alpha_n = n\frac{\pi}{a} \qquad \beta_m = m\frac{\pi}{b} \qquad \gamma_{mn} = \sqrt{\alpha_n^2 + \beta_m^2} \tag{20}$$

Similarly, displacements in the direction of the axis $x = u(t)$, axis $y = v(t)$ are determined from:

$$u = -z\varphi_x - \frac{16}{abc}\frac{F_0}{\rho h}\sum_{m=1}^{\infty}\sum_{n=1}^{\infty}\frac{J_1(\gamma_{mn}c)}{\gamma_{mn}}\frac{\alpha_n}{\omega_{mn}^2}\sin\alpha_n x_F \sin\beta_m y_F \cos\alpha_n x \sin\beta_m y \sin^2\frac{\omega_{mn}}{2}t \tag{21}$$

$$v = -z\varphi_y = -\frac{16}{abc}\frac{F_0}{\rho h}\sum_{m=1}^{\infty}\sum_{n=1}^{\infty}\frac{J_1(\gamma_{mn}c)}{\gamma_{mn}}\frac{\beta_m}{\omega_{mn}^2}\sin\alpha_n x_F \sin\beta_m y_F \sin\alpha_n x \cos\beta_m y \sin^2\frac{\omega_{mn}}{2}t$$

By deriving (18, 21), the relations for the velocities in the axis direction x, y, z are obtained:

$$\dot{w} = -\frac{8z}{abc}\frac{F_0}{\rho h}\sum_{m=1}^{\infty}\sum_{n=1}^{\infty}\frac{J_1(\gamma_{mn}c)}{\gamma_{mn}}\frac{\sin\alpha_n x_F \sin\beta_m y_F}{\omega_{mn}}\sin\alpha_n x \sin\beta_m y \sin\omega_{mn}t$$

$$\dot{u} = -\frac{8z}{abc}\frac{F_0}{\rho h}\sum_{m=1}^{\infty}\sum_{n=1}^{\infty}\frac{J_1(\gamma_{mn}c)}{\gamma_{mn}}\frac{\alpha_n}{\omega_{mn}}\sin\alpha_n x_F \sin\beta_m y_F \cos\alpha_n x \sin\beta_m y \sin\omega_{mn}t \tag{22}$$

$$\dot{v} = \frac{8z}{abc}\frac{F_0}{\rho h}\sum_{m=1}^{\infty}\sum_{n=1}^{\infty}\frac{J_1(\gamma_{mn}c)}{\gamma_{mn}}\frac{\beta_m}{\omega_{mn}}\sin\alpha_n x_F \sin\beta_m y_F \sin\alpha_n x \cos\beta_m y \sin\omega_{mn}t$$

Similarly, by substituting relation (18) into (8) and adjusting, the rotation angles of the tangents are obtained φ_x, φ_y in point x, y.

By substituting into (13) using equation (16), the relations for bending stresses σ_x, σ_y, and shear stresses from the bending moment ($\tau_{yx} = \tau_{xy}$) and shear stresses from shear forces (τ_{xz} and τ_{yz}) are obtained after adjustments, see e.g. [13].

2.1.2 Flüegge model

The Flüegge model (mF) of a thin plate differs from the Kirchhoff model (mK) by respecting the effect of shear, i.e. that it introduces shear corrections, but does not respect the effect of moments of inertia. Since $\partial^2\varphi_x/\partial t^2 = 0$ and $\partial^2\varphi_y/\partial t^2 = 0$, the second and third equations (17) change back to equations of moment static balance.

Displacements (12a, 12b) in the direction of the axes $x = u(t)$, $y = v(t)$, $z = w(t)$ caused by the impact load then have the form for the axis $z = w(x, y, t)$.

$$w(x, y, t) = \frac{16}{abc}\frac{F_0}{\rho h}\sum_{m=1}^{\infty}\sum_{n=1}^{\infty}\frac{J_1(\gamma_{mn}c)}{\gamma_{mn}}\sin\alpha_n x_F \sin\beta_m y_F \sin\alpha_n x \sin\beta_m y \sin^2\frac{\omega_F}{2}t \tag{23}$$

For axis $x = u(x, y, z, t)$ and $y = v(x, y, z, t)$ using equations (9, 10) we get relations:

$$u(x, y, z, t) = -z\varphi_x = -\frac{16}{abc}\frac{F_0}{\rho h}\sum_{m=1}^{\infty}\sum_{n=1}^{\infty}\frac{J_1(\gamma_{mn}c)}{\gamma_{mn}\omega_F^2}b_2\sin\alpha_n x_F \sin\beta_m y_F \cos\alpha_n x \sin\beta_m y \sin^2\frac{\omega_F}{2}t \tag{24}$$

$$v(x, y, z, t) = -z\varphi_y = -\frac{16}{abc}\frac{F_0}{\rho h}\sum_{m=1}^{\infty}\sum_{n=1}^{\infty}\frac{J_1(\gamma_{mn}c)}{\gamma_{mn}\omega_F^2}b_1\sin\alpha_n x_F \sin\beta_m y_F \sin\alpha_n x \cos\beta_m y \sin^2\frac{\omega_F}{2}t$$

Where:

$$\gamma_{mn} = \sqrt{\alpha_n^2 + \beta_m^2} \qquad \alpha_n = n\frac{\pi}{a} \qquad \beta_m = m\frac{\pi}{b} \qquad \omega_F = a_{11} + a_{12}b_2 + a_{13}b_1 \tag{25a}$$

$$D_x = \frac{E_x h^3}{12(1-\mu_{yx}\mu_{xy})} = D_y = \frac{E_y h^3}{12(1-\mu_{yx}\mu_{xy})} = D = \frac{Eh^3}{12(1-\mu^2)} \qquad D_{xy} = \frac{G_{xy}h^3}{12}$$

For the isotropic material of the plate, it is assumed that the stiffness modules $D = D_x = D_y$, elasticity $E = E_x = E_y$ and the viscosity coefficients of the material $\mu = \mu_x = \mu_y$.

We determine the coefficients a and b from the relations for ω_F calculation:

$$a_{11} = \frac{G_{xz}k}{\rho}\alpha_n^2 + \frac{G_{yz}k}{\rho}\beta_m^2 \qquad a_{12} = \frac{G_{xz}k}{\rho}\alpha_n \qquad a_{13} = \frac{G_{yz}k}{\rho}\beta_m$$

$$a_{21} = a_{13}\frac{12}{h^2} \qquad a_{22} = \frac{12}{\rho h^3}(G_{xy}hk + D_x\alpha_n^2 + D_{xy}\beta_m^2) \qquad a_{23} = \frac{12}{\rho h^3}(D_x\mu_{xy} + D_{xy})\alpha_n\beta_m$$

(25b)

$$a_{31} = a_{13}\frac{12}{h^2} \qquad a_{32} = \frac{12}{\rho h^3}(D_y\mu_{yx} + D_{xy})\alpha_n\beta_m \qquad a_{33} = \frac{12}{\rho h^3}(G_yhk + D_y\beta_m^2 + D_{xy}\alpha_n^2)$$

$$b_1 = \frac{a_{22}a_{31} - a_{32}a_{21}}{a_{23}a_{32} - a_{22}a_{33}} \qquad b_2 = \left(\frac{a_{21}}{a_{22}} + \frac{a_{23}}{a_{22}}b_1\right)$$

Where:

k…Dimensionless coefficient respecting the course of the shear stress [-].

The velocities in the directions of individual axes are determined by derivation (23, 24) according to time and adjustment.

$$\dot{w}(x, y, t) = \frac{8F_0}{abch\rho}\sum_{m=1}^{\infty}\sum_{n=1}^{\infty}\frac{J_1(\gamma_{mn}c)}{\gamma_{mn}\omega_F^2}\sin\alpha_n x_F \sin\beta_m y_F \sin\alpha_n x \sin\beta_m y \sin^2\omega_F t$$

$$u(x, y, z, t) = -\frac{8zF_0}{abch\rho}\sum_{m=1}^{\infty}\sum_{n=1}^{\infty}\frac{J_1(\gamma_{mn}c)}{\gamma_{mn}\omega_F^2}b_2\sin\alpha_n x_F \sin\beta_m y_F \cos\alpha_n x \sin\beta_m y \sin^2\omega_F t \qquad (26)$$

$$\dot{v}(x, y, z, t) = -\frac{8zF_0}{abch\rho}\sum_{m=1}^{\infty}\sum_{n=1}^{\infty}\frac{J_1(\gamma_{mn}c)}{\gamma_{mn}\omega_F^2}b_1\sin\alpha_n x_F \sin\beta_m y_F \sin\alpha_n x \cos\beta_m y \sin^2\omega_F t$$

Equivalently, from relations (8, 9) by substituting from (23) and modifying, we get the relations for rotation of the tangents φ_x, φ_y:

$$\varphi_x(x, y, t) = \frac{\partial w}{\partial x} = \frac{16F_0}{abch\rho}\sum_{m=1}^{\infty}\sum_{n=1}^{\infty}\frac{J_1(\gamma_{mn}c)}{\gamma_{mn}\omega_F^2}b_2\sin\alpha_n x_F \sin\beta_m y_F \cos\alpha_n x \sin\beta_m y \sin^2\frac{\omega_F}{2}t$$

(27)

$$\varphi_y(x, y, t) = \frac{\partial w}{\partial y} = \frac{16F_0}{abch\rho}\sum_{m=1}^{\infty}\sum_{n=1}^{\infty}\frac{J_1(\gamma_{mn}c)}{\gamma_{mn}\omega_F^2}b_1\sin\alpha_n x_F \sin\beta_m y_F \sin\alpha_n x \cos\beta_m y \sin^2\frac{\omega_F}{2}t$$

3 Methods of solution

The article deals with the solution of propagation of longitudinal and transverse waves in a thin isotropic plate. As mentioned above, a thin isotropic plate is solved. Kirchhoff's and Flüegge's geometric models are compared, the plate material is assumed to be isotropic.

3.1 Methodology

Wave propagation is solved analytically in the MATLAB program. Individual geometric models were programmed and the courses of displacements and velocities in individual axes (x, y, z) were determined.

The following conditions were set for the solution:

- The velocity of wave propagation in the given material (depends on the material and dimensions of the plates) was determined, both in the longitudinal and transverse directions.

- The maximum calculation time is determined by the speed of wave propagation in a given direction (longitudinal and transverse wave) and the shortest distance to the edge (the wave will be reflected at the support place

and the wave will be deformed - it was not already monitored).

- The plate dimensions were selected ($a \times b \times h$, where $a = 200$ mm, $b = 100$ mm, $h = 2$ mm).

- The plate is supported around the entire circumference in the width of 5 mm (the original dimension of the plate before is $210 \times 110 \times 2$ mm).

- The plate load is the impact force at the center of the plate, the center of the impact is at the geometric center of the plate.

- The magnitude of the impact force was set at $F(t) = 1$ N.

- The distance at which the deflections were monitored and the velocities were determined was at 20 mm from the center of the impact.

- Due to the fact that it is not possible to achieve a point impact of the force during the experiment, the radius of the impact body of the force was chosen $c = 2.5$ mm.

The velocity of wave propagation in the transverse and longitudinal directions was determined (a transverse wave has a velocity of 0.5 of the velocity of a longitudinal wave). The size of the impact force does not affect the course (shape) of wave propagation (deflections, velocities, stress), but it does affect their size.

The course of the propagating shock wave (deformation, deformation rate) was determined according to the relationships given in section 2. For the assessment of wave propagation, only the first wave (deformation, velocity, acceleration, stress) before it reaches the interface is important (plate edges, weaving, support, etc.). The interference will occur after reflection.

3.2 Results and discussion

An isotropic aluminum plate Al 99.5 was chosen for the solution (chemical composition: Al 99.56%, B 0.001%, Bi 0.0002%, Ca 0.002%, Cd 0.0001%, Cr 0.001%, Cu 0.0018%, Fe 0.3097%, Ga 0.0084%, Hg 0.0002%, Mg 0.0012%, Mn 0.0036%, Na 0.0002%, Ni 0.0034%, P 0.0004%, Pb 0.0011%, Si 0.0721%, Sn 0.0008%, Ti 0.0187%, V 0.0096%, Zn 0.0025%, others 0.0038%). A sheet with a thickness of 2 mm was produced from the mentioned material by unidirectional cold rolling. Test plates with the dimensions $a \times b \times h$ ($210 \times 110 \times 2$ mm) and test rods for the tensile test were cut from the sheet, so that they were not affected by heat.
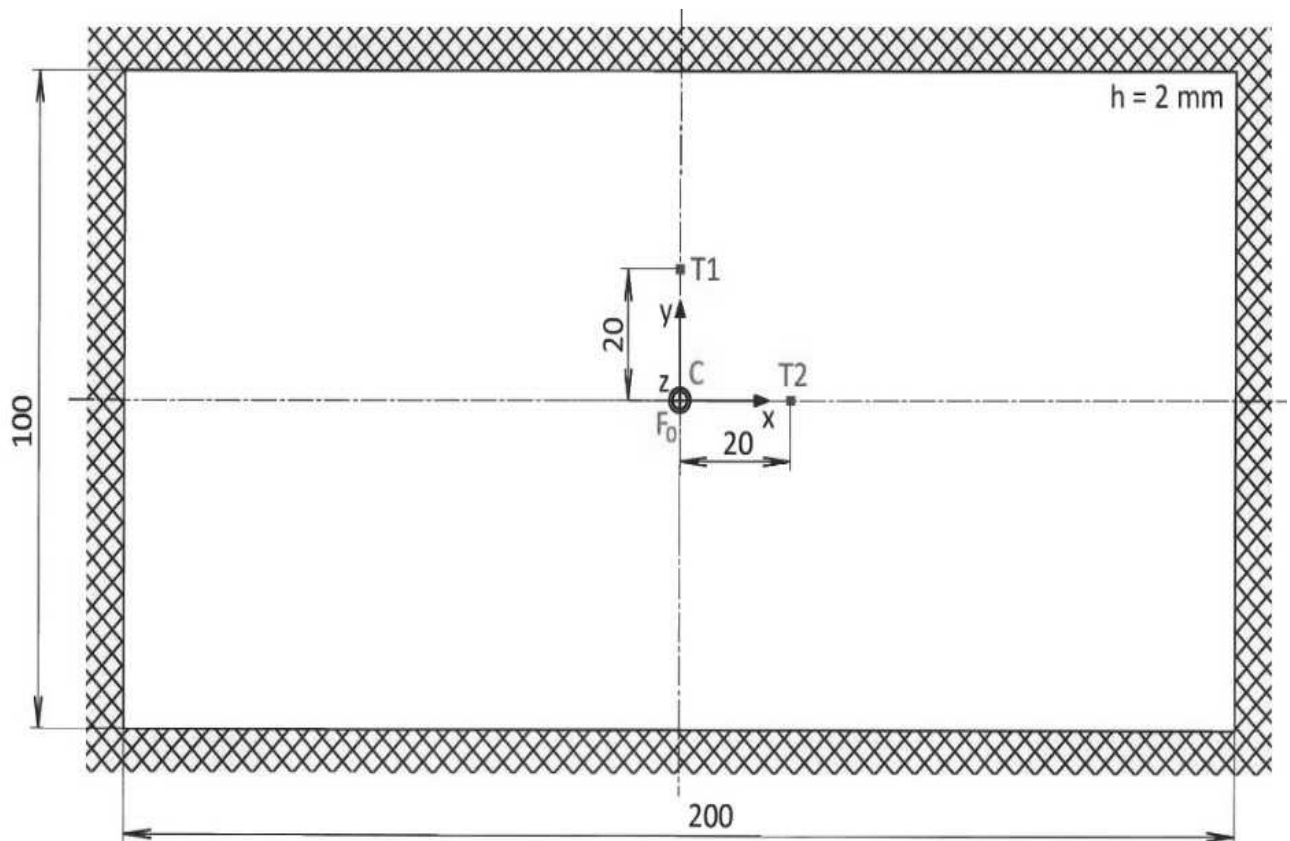

Fig. 5 *Scheme of a supported plate (T1 (0, 20), T2 (20, 0), - observed points, C - geometric center of the plate, center of impact, F_0 - impact force, x, y, z - axes passing through the geometric center of the plate)*

A tensile test was performed on the Inspekt 100 kN tensile testing machine (see Fig. 6).
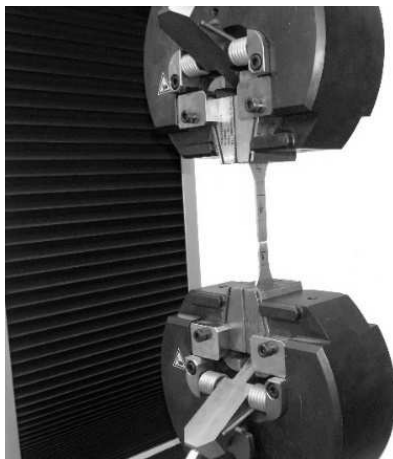

The measurement was repeated 10 times (the strain diagram including average values is in Fig. 7) and statistically evaluated. The resulting value of the tensile modulus of elasticity was used in the calculations.

E	7	GPa
F_{max}	5225	N
R_m	124	MPa
$F_{p0.2}$	5169	N
$R_{p0.2}$	123	MPa
A	12.2	%

***Fig. 7** A broken test rod in a tensile test machine*

***Fig. 6** A broken test rod in a tensile test machine*

Material properties of the plate are given in Tab. 1 [23-27].

Tab. 1 *Material properties of the plate*

Property	Symbol	Unit	Value
Young's module	$E = E_x = E_y = E_z$	Pa	7×10^{-10}
Poisson's ratio	μ	-	0.34
Density	ϱ	kgm^{-3}	2699

To verify the statement that the magnitude of the shock force does not affect the time course of shock wave propagation in isotropic material, the calculation of displacement propagation in the direction of the z axis ($w(t)$) was performed for three magnitudes of the shock force ($F_0 = 1, 5, 10$ N) for the Kirchhoff plate model and a mutual comparison was made (Fig. 8).
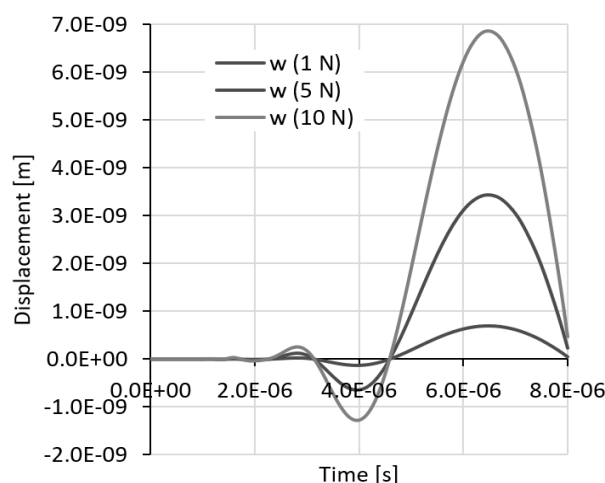

***Fig. 8** Comparison of the displacement (deformation) w of a thin plate in the direction of the z axis depending on the magnitude of the impact force (Kirchhoff's geometric model of the plate, Hooke's material model)*

3.2.1 Kirchhoff's Model – Results of the Solution

The propagation of the wave in the direction of the x, y and z axes is monitored, both the magnitude of

the deformation and its rate. It follows from the theory that the velocity of propagation of the shock wave in the longitudinal direction is twice the velocity of the transverse wave. For isotropic materials, it is assumed that the wave propagation velocities in the x and y axis directions are equal.

Fig, 9a) shows the propagation of the deformation of the thin plate in the direction of the x and y axes at a distance of 20 mm from the impact center, i.e. at points T1 (0, 20) and T2 (20, 0).

***Fig. 9** Displacement in the direction of the x and y axes (a) and in the direction of the z axes (b) for point T1 and T2 as a function of time (Kirchhoff)*

Tab. 2 *Displacement of wave in x (u) and y (v) axis direction in points T1, T2 (Kirchhoff)*

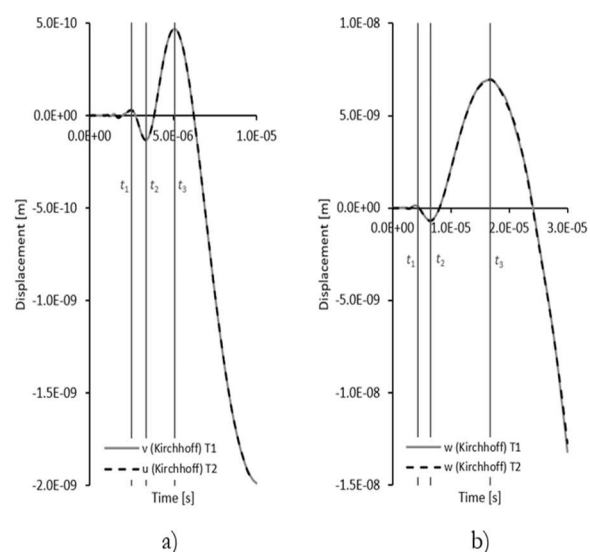| Symbol	Time	Displacement		Comparison	
		u (T2)	v (T1)	Col. 4 − Col. 3	(Col. 5 / Col. 3)·100
	[s]	[m]	[m]	[m]	[%]
1	2	3	4	5	6
t_1	2.500×10^{-6}	0.284×10^{-10}	0.284×10^{-10}	0.000×10^{-10}	0.000
t_2	3.400×10^{-6}	-1.338×10^{-10}	-1.337×10^{-10}	0.001×10^{-10}	-0.075
t_3	5.100×10^{-6}	4.662×10^{-10}	4.670×10^{-10}	0.008×10^{-10}	0.172

The courses of displacement in the longitudinal direction u in the direction of the x axis and displacement v in the direction of the y axis are identical. In the figure (Fig. 9a) both lines overlap (there is no visible difference). As can be seen from Fig. 9a) and Tab. 2, the displacement differences in the direction of the x-axis (u) and in the direction of the y-axis (v) are very small. The biggest difference is at time $t_3 = 5.1 \times 10^{-6}$ s and that is 0.172 %, which is very little. It can be stated that the agreement is very good.

The differences are believed to be due to inaccuracies in the determination of the Bessel function and the cos and sin functions.

Displacement courses in the z-axis (w - see Fig. 9b) and their numerical values at selected times are shown in Table 3. From Fig. 9b) and Tab. 3, a very good agreement of vertical displacements in both points (T1, T2) can be seen. The difference reaches its maximum value at time $t_3 = 16.70 \times 10^{-6}$ s.

Tab. 3 *Displacement of wave in z (w) axis direction in points T1, T2 (Kirchhoff)*

Symbol	Time	Displacement		Comparison	
		w (T2)	w (T1)	Col. 4 − Col. 3	(Col. 5 / Col. 3)·100
	[s]	[m]	[m]	[m]	[%]
1	2	3	4	5	6
t_1	0.430×10^{-5}	0.901×10^{-10}	0.901×10^{-10}	0.000×10^{-10}	0.000
t_2	0.650×10^{-5}	-6.864×10^{-10}	-6.860×10^{-10}	0.004×10^{-10}	-0.058
t_3	1.670×10^{-5}	69.650×10^{-10}	69.380×10^{-10}	-0.270×10^{-10}	-0.388

It can be stated that the deformation is propagated uniformly in the x, y, z axis. The slight differences are beyond possible mathematical errors (determining the magnitude of the sin and cos functions).

As mentioned above, waves in a thin plate propagate in the direction of the x, y axis at twice the velocity than in the direction of the z axis. The time trends of the velocities (points T1 and T2) are presented in the Fig, 10a). Numerical values of speed $\dot{u}$ and $\dot{v}$ at selected times and points are in Tab. 4 in the direction of the x axis.

As can be seen from Tab. 4, the difference in wave speed propagation is the highest at time $t_3 = 4.100 \times 10^{-6}$ s, which is probably due to the instability of the calculation (the already mentioned determination of the size of the cosinus and sinus functions, the inaccuracy of the Bessel function calculation, etc.). At other times, the course of the wave propagation velicity in both directions (x, y) shows good agreement.
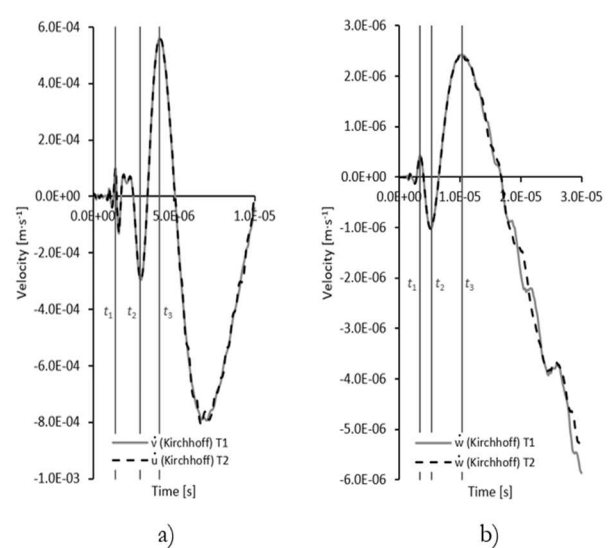
Fig. 10 *Velocity time trend in the x and y axes direction (a) and in the z axis direction (b) for point T1 and T2 (Kirchhoff)*

Tab. 4 *Velocity of wave propagation in x (u̇) and y (v̇) axis direction in points T1, T2 (Kirchhoff)*

Symbol	Time	Velocity		Comparison	
		$\dot{u}$ (T2)	$\dot{v}$ (T1)	Col. 4 – Col. 3	(Col. 5 / Col. 3)·100
	[s]	[m.s^{-1}]	[m.s^{-1}]	[m.s^{-1}]	[%]
1	2	3	4	5	6
t_1	1.400×10^{-6}	0.975×10^{-4}	0.975×10^{-4}	0.000×10^{-4}	0.000
t_2	2.900×10^{-6}	-2.925×10^{-4}	-2.921×10^{-4}	0.004×10^{-4}	-0.137
t_3	4.100×10^{-6}	5.578×10^{-4}	5.594×10^{-4}	0.016×10^{-4}	0.287

The course of the speed in the transverse direction $\dot{w}$ (in the z axis) - see Fig, 10b) shows a very good agreement in both mutually perpendicular points T1 and T2 – Tab. 5.

Tab. 5 *Velocity of wave propagation in z (ẇ) axis direction in points T1, T2 (Kirchhoff)*

| Symbol	Time	Velocity		Comparison	
		$\dot{w}$ (T2)	$\dot{w}$ (T1)	Col. 4 – Col. 3	(Col. 5 / Col. 3)·100
	[s]	[m.s^{-1}]	[m.s^{-1}]	[m.s^{-1}]	[%]
1	2	3	4	5	6
t_1	0.340×10^{-5}	0.430×10^{-6}	0.430×10^{-6}	0.000×10^{-6}	0.000
t_2	0.530×10^{-5}	-0.993×10^{-6}	-0.995×10^{-6}	-0.002×10^{-6}	0.201
t_3	1.030×10^{-5}	2.454×10^{-6}	2.421×10^{-6}	-0.033×10^{-6}	-1.345

As can be seen from Fig. 10b) and Tab. 5, the wave propagation velocities in the transverse direction at times t_1 and t_2 are the same. Small variations in time t_3 can be attributed to rounding in the calculations. Compared to the velocity propagation in the longitudinal direction (x and y axes), the propagation velocity in the transverse direction (z axis) is half (see longer times of local extrema in Tab. 4 and Tab. 5).

3.2.2 Flüegge's Model – Results of the Solution

A similar calculation was performed for Flüegge model as for the Kirchhoff model. Displacement relations (23, 24) and equations (25a, b) were used. The velocities were determined from relations (26). The analytical calculation was again performed in the MATLAB program.

Fig. 11a) shows the course of displacements in the x and y directions during shock loading of the plate in the geometric center (see Fig. 5). It can be seen from the course that the deformation propagates uniformly from the point of impact in all directions of the xy plane – in circles. Numerical values of local extremes at times t_1, t_2 and t_3 are shown in Tab. 6. At time t_1,

the difference in deviation values is less than 3.5 %, which is a good agreement. The difference can be attributed to rounding inaccuracies in the calculation.
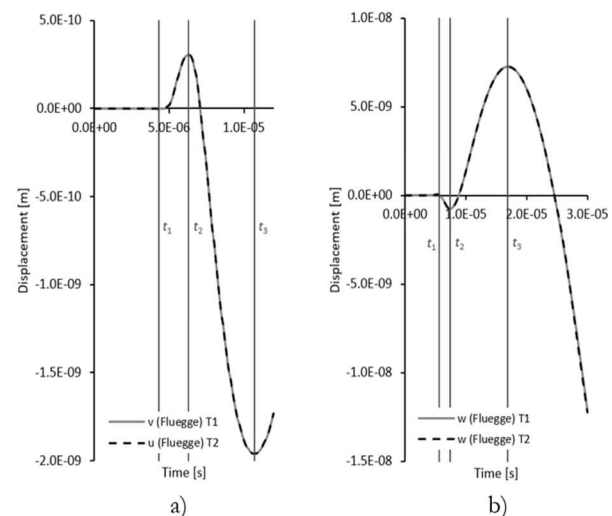
Fig. 11 *Displacement in the direction of the x and y axes (a) and in the direction of the z axes for point T1 and T2 as a function of time (Flüegge)*

Tab. 6 *Displacement of wave in x (u) and y (v) axis direction in points T1, T2 (Flüegge)*

Symbol	Time	Displacement		Comparison	
		u (T2)	v (T1)	Col. 4 – Col. 3	(Col. 5 / Col. 3)·100
	[s]	[m]	[m]	[m]	[%]
1	2	3	4	5	6
t_1	0.430×10^{-5}	-0.029×10^{-10}	-0.028×10^{-10}	0.001×10^{-10}	-3.448
t_2	0.630×10^{-5}	3.079×10^{-10}	3.079×10^{-10}	0.000×10^{-10}	0.000
t_3	1.070×10^{-5}	-19.600×10^{-10}	-19.600×10^{-10}	0.000×10^{-10}	0.000

Fig. 11b) shows the course of propagation of transverse displacement in the direction of the z axis at points T1, T2. The displacement trend shows a very good agreement. As can be seen in Tab. 7, the difference in lateral displacement is less than 0.6 % at time t_1. The displacement trend is the same at both points (T1, T2). The slight deviation can again be attributed to the effect of rounding during the calculation.

Tab. 7 *Displacement of wave in z (w) axis direction in points T1, T2 (Flüegge)*

Symbol	Time	Displacement		Comparison	
		w (T2)	w (T1)	Col. 4 – Col. 3	(Col. 5 / Col. 3)·100
	[s]	[m]	[m]	[m]	[%]
1	2	3	4	5	6
t_1	0.560×10^{-5}	0.169×10^{-10}	0.168×10^{-10}	$-0{,}001 \times 10^{-10}$	-0.592
t_2	0.740×10^{-5}	-7.564×10^{-10}	-7.565×10^{-10}	-0.001×10^{-10}	0.013
t_3	1.690×10^{-5}	72.570×10^{-10}	72.570×10^{-10}	0.000×10^{-10}	0.000

Fig. 12 shows the course of the velocity of the propagating wave in the xy plane (Fig. 12a) and in the z axis (Fig. 12b) at points T1, T2. A very good agreement can be seen from the pictures. In Fig. 12b) after time t_3, the influence of the reflected wave from the interface is already visible. It is evident from this that the original and reflected wave will be superimposed and the course will be significantly influenced. In the xy plane, where the speed of the propagating wave is twice that of the transverse direction, the influence of the reflected wave is not noticeable in the monitored time period (the interface distance is at least 25× greater than in the transverse direction, the monitored time is too short).

As can be seen from Tab. 8, the difference in velocity wave propagation is greatest at time t_1, less than 0.4 %, which can again be attributed to the effect of rounding. Tab. 9 shows the local speed extremes in the transverse direction at points T1, T2. The agreement on both points is very good.
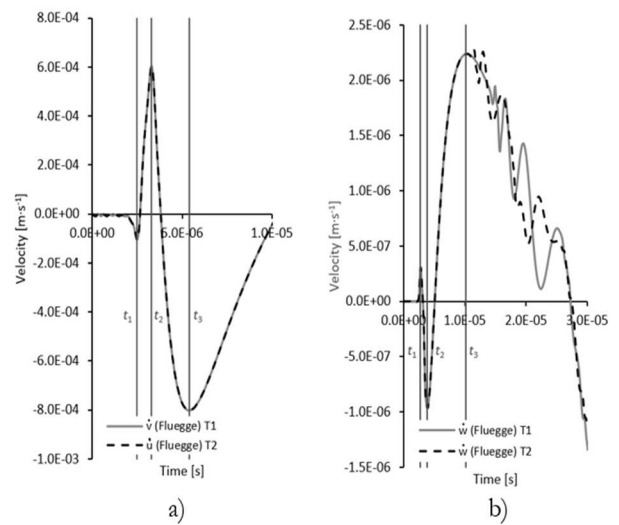

Fig. 12 *Velocity in the direction of the x and y axes (a) and in the direction of the z axes for point T1 and T2 as a function of time (Flüegge)*

Tab. 8 *Velocity of wave propagation in x (u) and y (v) axis direction in points T1, T2 (Flüegge)*

Symbol	Time	Velocity		Comparison	
		$\dot{u}$ (T2)	$\dot{v}$ (T1)	Col. 4 – Col. 3	(Col. 5 / Col. 3)·100
	[s]	[m.s^{-1}]	[m.s^{-1}]	[m.s^{-1}]	[%]
1	2	3	4	5	6
t_1	2.500×10^{-6}	-1.053×10^{-4}	-1.049×10^{-4}	0.004×10^{-4}	-0.380
t_2	3.300×10^{-6}	6.034×10^{-4}	6.036×10^{-4}	0.002×10^{-4}	0.033
t_3	5.400×10^{-6}	-8.034×10^{-4}	-8.032×10^{-4}	0.002×10^{-4}	-0.025

Tab. 9 *Velocity of wave propagation in z (ẇ) axis direction in points T1, T2 (Flüegge)*

Symbol	Time	Velocity		Comparison	
		$\dot{w}$ (T2)	$\dot{w}$ (T1)	Col. 4 – Col. 3	(Col. 5 / Col. 3)·100
	[s]	[m.s^{-1}]	[m.s^{-1}]	[m.s^{-1}]	[%]
1	2	3	4	5	6
t_1	0.270×10^{-5}	0.307×10^{-6}	0.307×10^{-6}	0.000×10^{-6}	0.000
t_2	0.380×10^{-5}	-0.963×10^{-6}	-0.963×10^{-6}	0.000×10^{-6}	0.000
t_3	1.020×10^{-5}	2.237×10^{-6}	2.236×10^{-6}	-0.001×10^{-6}	-0.045

3.2.3 Comparison of Kirchhoff's and Flüegge's Models

From the above calculations, it follows that when comparing the results performed according to the geometric model of Kirchhoff and Flüegge using the material model of Hooke, we can focus on the comparison of

- Shape of wave propagation in an isotropic material.
- From the comparison of maximum values depending on time.

The courses of deflections and speeds are compared, both in the longitudinal (x, y axes) and transverse (z axis) directions. Obviously, the maximum values will differ since the two models are based on different assumptions. Flüegge's model extends the original Kirchhoff theory, which considers only vertical displacements and their corresponding inertial effects, by the effect of shear on the resulting vertical displacement.

Considering that this is an isotropic material (see the results above), we deal with the comparison of longitudinal and transverse displacement, velocity in the longitudinal and transverse directions only at point T1.

Fig. 13 compares the displacement (deformation) propagation courses in the y direction (Fig. 13a) and in the transverse direction (Fig. 13b – z axis).
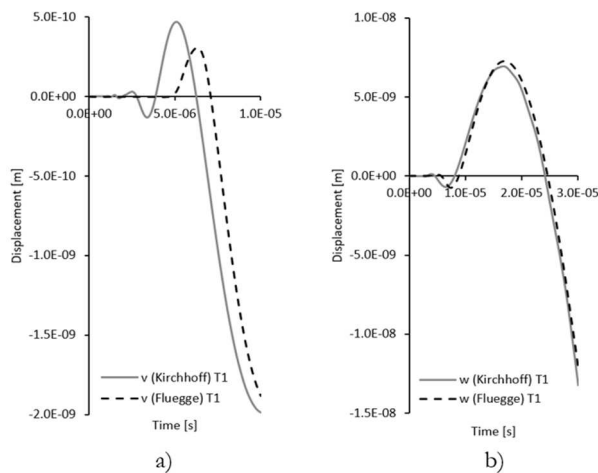

Fig. 13 *Displacement course in the y-axis (a) and in the z-axis (b) for the Kirchhoff and Flüegge model at point T1*

From the course of displacements in the y-axis (Fig. 13a), it can be seen that at the beginning, local extremes (positive and negative) are visible in Kirchhoff's case, they are quite significant, while in Flüegge's case, only the positive extreme is noticeable. The significant positive extreme in Kirchhoff and Flüegge are similar in shape, but in Flüegge it is lower and shifted to a longer time. It is probably caused by the influence of the distribution of the energy of the impact on the deformation and the shear force.

According to Kirchhoff's model, the deformation in the direction of the y axis reaches its maximum positive value at a time of 5.10×10^{-6} s and that is 4.670×10^{-10} m, with Fluegge's model the deflection is 3.079×10^{-10} m at a time of 6.30×10^{-6} s.

In the direction of the z axis, for the Kirchhoff model, the maximum positive deflection is 6.938×10^{-10} m at a time of 1.67×10^{-5} s, for the Flüegge model it is 7.257×10^{-10} m at a time of 1.69×10^{-5} s.

Fig. 14 shows a comparison of wave propagation speeds in the direction of the y and z axes for the above models.
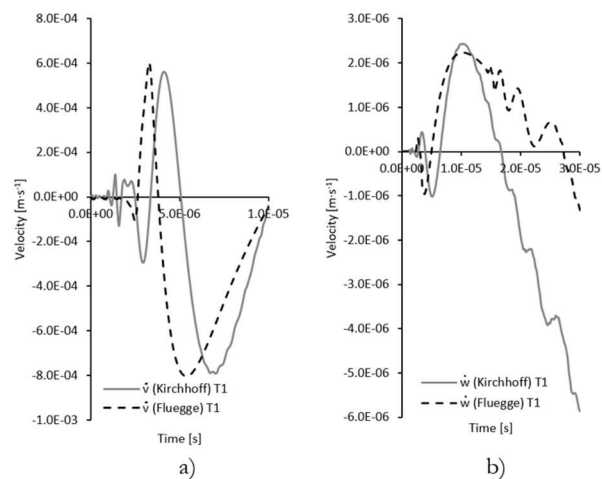

Fig. 14 *Course of velocities in the y-axis (a) and in the z-axis (b) for the Kirchhoff and Flüegge model at point T1*

It can be seen from Fig. 14 that, in contrast to the deformation propagation (Fig. 13), the speed in the Flüegge model is higher in both directions (y and z), i.e. it reaches the maximum positive value in a shorter time than in the Kirchhoff model. The positive maximum of 5.594×10^{-4} m.s^{-1} is reached by the speed $\dot{v}$ for the Kirchhoff model in time 4.10×10^{-6} s, for the Flüegge model in time 3.30×10^{-6} s the value is 6.036×10^{-4} m.s^{-1}. The speed $\dot{w}$ in the direction of the z axis is 2.421×10^{-6} m.s^{-1} at time 1.30×10^{-5} s for the Kirchhoff model, the speed value is 2.236×10^{-6} m.s^{-1} at time t_1 for Fluegge's model. 02×10^{-5} s. The shape of the velocity curve $\dot{v}$ in the direction of the y-axis is similar for both models. In the direction of the z-axis it ($\dot{w}$) is also similar, with the fact that, as in the course of the deformation will show the influence of the reflected wave in the observed time.

4 Conclusion

The article deals with the analytical calculation of the propagation of deformations and velocities in a thin circumferentially supported isotropic rectangular plate under impact loading. An impact force of 1 N (considered Heaviside jump) was applied to create

impact of a body radius of 2.5 mm with a spherical end to the geometric center of the face of the plate.

A brief analytical solution is presented and its application for the calculation for each geometric model (Kirchhoff's and Fluegge's) was performed in the MATLAB program. Hooke's material model was considered for both geometric models. The result of the calculation is the course of deformations and velocities in the direction of the x, y, z axes at points T1, T2, which are at a distance of 20 mm from the center of the impact in the direction of the x and y axes respectively.

From the evaluation of the results, it follows that for the Kirchhoff model the course of deformation and velocity as a function of time is essentially the same at both monitored points, slight deviations can be attributed to rounding during the calculation.

In Fluegge's geometric model, which, in contrast to Kirchhoff's geometric model, considers the effect of shear on the resulting vertical displacement, the coincidence of the course of deformations and velocities as a function of time in both monitored points T1 and T2 is almost identical. The slight differences have the same causes as in Kirchhoff's geometric model.

From the comparison of the propagation of deformations of both geometric models (see Fig. 13), it follows that the deformation according to the Flüegge model has time delay in the propagation of deformation according to the Kirchhoff model. Fig. 13a) shows the course of the deformation at point T1 (in the y axis), from which it is evident that not only a time shift occurs, but also a reduction in the amplitude of the deflection in the Flüegge model. This is due to the fact that the calculation also considers the effect of shear forces and therefore to a loss of energy. Regarding the displacement in the z-axis (Fig. 13b), a slight delay is also evident. As for the amplitude of the displacement, it is slightly larger with the Flüegge model. These differences are considerably smaller than the differences in longitudinal displacement propagation, which is mainly a consequence of the shorter path (only 2 mm versus 20 mm in the y-axis) and the slower wave propagation in the transverse direction.

In contrast to the above, the velocity propagation is slower for Kirchhoff's geometric model than for Fluegge's (Fig. 14). As for the velocity amplitude, the Flüegge model has a higher velocity in the longitudinal direction (Fig. 14a), while the Kirchhoff model achieves higher values in the transverse direction (Fig. 14b).

References

[1] ABRATE, S. (2011). *Impact Engineering of Composite Structures*, 1. ed. CISM: Springer – Verlag Wien, 403 p. ISBN 978-3-7091-0522-1.

[2] MOLNÁR, D. BLATNICKÝ, M., DIŽO, J. (2022) Comparison of Analytical and Numerical Approach in Bridge Crane Solution. In: *Manufacturing Technology*, Vol. 22, No. 2, pp. 192-199, ISSN 1213–2489. DOI: 10.21062/mft.2022.018

[3] ZAWADA-MICHAŁOWSKA, M., PIEŚKO, P., LEGUTKO, S. (2023) Effect of the Cutting Tool on the Quality of a Machined Composite Part. In: *Manufacturing Technology*, Vol. 23, No. 6, pp. 870-879, ISSN 1213–2489. DOI: 10.21062/mft.2023.107

[4] KHORSHIDI, K. (2011). Elasto-Plastic Response of Impacted Moderatly Thick Rectangular Plates with Different Boundary Conditions, In: *Procedia Engineering* Vol. 10, pp. 1742 – 1747.

[5] WANG, J., DONG, S., PANG, S. D., YU, X., HAN, B., OU, J. (2022). Tailoring Anti-Impact Properties of Ultra-High Performance Concrete by Incorporating Functionalized Carbon Nanotubes. In: *Engineering*, Vol. 18, pp. 232–245. https://doi.org/10.1016/j.eng.2021.04.030

[6] VANAM, B., INALA, R. (2012). Static analysis of an isotropic rectangular plate using finite element method (FEM). In: *Mech. Eng.*, Vol. 4, pp. 148–162.

[7] VOLEK, J. (2000). Nestacionární *Napjatost Tenké Desky Vyvolané Příčnou Osamělou Silou;* Bulletin vědeckých, výzkumných a pedagogických prací ústavu za rok 2000, Ústav techniky a řízení výroby, UJEP: Ústí nad Labem, Czech Republic.

[8] MOHANTY, S., C., RAMU, I. (20212). Study of Free Vibration Analysis of Rectangular Plate Structures Using Finite Element Method. In: *Procedia Eng.*, Vol. 38, pp. 2758–2766.

[9] KLIMENDA, F.; SOUKUP, J. (2017). Modal Analysis of Thin Aluminium Plate. In: *Procedia Eng.,* Vol. 177, pp. 11–16. ISSN 1877-7058.

[10] DEUTSCH, A., EISENBERGER, M. (2022). Benchmark analytic in-plane vibration frequencies of orthotropic rectangular plates. In: *Journal of Sound and Vibration*, Vol. 541, 117248. https://doi.org/10.1016/j.jsv.2022.117248

[11] DARUS, M., I., Z., TOKHI, M., O. (2010). *Dynamical modelling and simulation of flexible rectangular isotropic plate structure using finite difference method*, United Kingdom, p. 6.

[12] GUO, H., ZHANG, K., LIN, T. R., ZHANG, B. (2023). Effect of ribs on vibration characteristics of cantilever plate. In: *Thin-Walled Structures*, Vol. 182, 110205. https://doi.org/10.1016/j.tws.2022.110205

[13] KLIMENDA, F.; SOUKUP, J.; RYCHLIKOVA, L.; SKOCILAS, J. (2022). Transverse Wave Propagation in a Thin Isotropic Plate Part I. In. *Appl. Sci.,* Vol. 12, 2493. https://doi.org/10.3390/app12052493

[14] WU, J., J., TING, T., C., T., BARNETT, D., M. (1991). *Modern theory of anisotropic elasticity and applications*, SIAM, Philadelphia,

[15] NIAZ, M., NIKKHOO, A. (2015). Inspection of a Rectangular Plate Dynamics Under a Moving Mass With Varying Velocity Utilizing BCOPs. In: *Latin American Journal of Solids and Structures*, Vol. 12, pp. 317-332.

[16] MAHABADI, R., K., SHAKERI, M., PAZHOOH, M., D. (2016). Free Vibration of Laminated Composite Plate with Shape Memory Alloy Fibers. In: *Latin American Journal of Solids and Structures*, Vol. 13, pp. 314-330.

[17] CHIKER, Y., MOURAD, B., BOUAZIZ, S., MOULOUD, G., AMAR, M., B., HADDAR, M. (2020). Free vibration analysis of hybrid laminated plates containing multilayer functionally graded carbon nanotube-reinforced composite plies using a layer-wise formulation. In: *Arch. Appl. Mech.,* Vol. 91, pp. 463–485.

[18] KARIMIMAHABADI, R., DANESHPAZHOOH, M., SHAKERI, M. (2021) On the free vibration and design optimization of a shape memory alloy hybrid laminated composite plate. In: *Acta Mech.*, Vol. 232, pp. 1–21.

[19] WANG, Z., MA, L. (2021). Effect of Thickness Stretching on Bending and Free Vibration Behaviors of Functionally Graded Graphene Reinforced Composite Plates. In: *Appl. Sci.,* Vol. 11, 11362. https://doi.org/10.3390/app112311362.

[20] HSU, M. H. (2003).Vibration Analysis of Isotropic and Orthotropic Plates with Mixed Boundary Conditions. Tamkang . In: *Sci. Eng.*, Vol. 6, pp. 217–226.

[21] WANG, Y., FAN, J., SHEN, X., LIU, X., ZHANG, J., REN, N. (2022). Free vibration analysis of stiffened rectangular plate with cutouts using Nitsche based IGA method. In: *Thin-Walled Structures,* Vol. 181, 109975. https://doi.org/10.1016/j.tws.2022.109975

[22] VAVRO J., JR., VAVRO, J., VAVROVA, A. (2019) Experimental and Numerical Modal Analysis of the Carbon Composite Plate Damaged by Cut. In: *Manufacturing Technology*, Vol. 19, No. 5, pp. 892-895, ISSN 1213–2489

[23] MICHNA, S., LUKAC, I., OCENASEK, V., KORENY, R., DRAPALA, J., SCHNEIDER, H., MISKUFOVA, A. and KOL. (2015). *Encyklopedie hliniku*, 1. vydani, Adin, s. r. o., Presov, 722 str., ISBN 80-89041-88-4

[24] MANEK, M., FUSEK, M. (2023). Comparison of measurement of aluminium alloy in high strain rate. In: *Journal of Mechanical Engineering*, Vol. 73, No. 99, pp. 99-106, SjF STU Bratislava, ISSN 2450-5471

[25] ZHANG, L., SONG, B., LIU, R., ZHAO, A., ZHANG, J., ZHUO, L., TANG, G., SHI, Y. (2020). Effects of Structural Parameters on the Poisson's Ratio and Compressive Modulus of 2D Pentamode Structures Fabricated by Selective Laser Melting. In: *Engineering,* Vol. 6, No. 1, pp. 56–67. https://doi.org/10.1016/j.eng.2019.06.009

[26] HRBÁČEK, P., VAŠIMA, M. (2022) Study of Light Transmission and Noise Attenuation Properties of Light Active Glass Materials. In: *Manufacturing Technology*, Vol. 22, No. 5, pp. 542-549, ISSN 1213–2489. DOI: 10.21062/mft.2022.062

[27] VAŠIMA, M., PÖSCHL, M., ZÁDRAPA, P. (2021) Influence of Rubber Composition on Mechanical Properties. In: *Manufacturing Technology*, Vol. 21, No. 2, pp. 261-269, ISSN 1213–2489. DOI: 10.21062/mft.2021.021